COMPARISON OF THE ABILITIES OF MULTIPLE ACOUSTIC TECHNIQUES FOR BUBBLE DETECTION

T G Leighton, D G Ramble and A D Phelps

Institute of Sound & Vibration Research, Southampton University, Highfield, Southampton SO17 1BJ, UK.

1. ABSTRACT

There exists a range of acoustic techniques for characterising bubble populations within liquids. Each technique has limitations, and complete characterisation of a population requires the sequential or simultaneous use of several, so that the limitations of each find compensation in the others. Here, nine techniques are deployed using one experimental rig, and compared to determine how accurately and rapidly they can characterise given bubble populations, specifically: (i) two stationary bubbles attached to a wire; and (ii) injected, rising bubbles.

2. INTRODUCTION

Bubble detection is required for many industrial [1], medical [2] and environmental [3] applications [4,5]. Throughout the range of acoustic techniques by which this can be achieved, there are inherent limitations: Some are appropriate only to relatively high, uniform, bubble population densities [6,7], where the inter-bubble spacing is very much less than the acoustic wavelength allowing homogeneous bulk properties to be assigned to the 'bubbly liquid' as a whole; others may be practicable only at low densities [8,9]. Several are prone to false triggering, in that some other object (e.g. a solid body, or a cluster of small bubbles [10]) may give the same signal as that obtained from a given bubble.

In water with ambient pressure p_0, an air bubble of radius R_0>~10 μm has a well-defined resonance frequency $f_0=\omega_0/2\pi \approx 0.01(\sqrt{p_0})/R_0$, and pulsates as a lightly-damped oscillator: On entrainment the pulsations generate an acoustic 'signature', an exponentially-decaying sinusoid, the frequency of which indicates the bubble size [11,12]. A few milliseconds after entrainment these passive emissions have decayed to below the level of the noise; however the bubble may still be driven, and active acoustic techniques exploit this acoustic resonance [6,7,13,14] through measurements of sound speed, attenuation, scattering, etc. At a particular frequency the acoustic response of a bubbly liquid is taken to be dominated by bubbles which are resonant with that frequency. The maximum number of different bubble sizes that can be measured at any one time is determined by the number of different frequencies investigated, which historically is usually one, but in notable cases has been four [13] or around nine [7]. However, even simple linear theory demonstrates that the acoustic scattering cross-section of the fundamental frequency is only a local, and not a global, maximum at resonance [15]: Bubbles very much larger than resonance size can geometrically scatter sound to a greater degree than can smaller, resonant bubbles. If an ultrasonic interrogating signal is employed, the frequency of which is very much higher than the resonances of any bubbles in the sample, geometric scattering can detect bubbles [16-18]: If MHz sound is, for example, employed to detect mm-sized bubbles, the small wavelengths involved (≈0.4 mm in water at 3.5 MHz) allow the bubble to be located, but do not accurately give bubble size. Geometric, non-resonant scattering relies on the acoustic impedance mismatch between the inhomogeneity and the surrounding liquid, and so is insensitive to the nature of the inhomogeneity, and in practice may not distinguish between bubbles and solid bodies of a similar size.

MULTIPLE ACOUSTIC TECHNIQUES FOR BUBBLE DETECTION

A bubble in an acoustic pressure field $P=A\cos\omega_p t$ tends to linear, low-amplitude oscillations if the driving amplitude A is small, or if the bubble is far from resonance. However, the high amplitude nonlinear pulsations of a resonant bubble will generate harmonics. For example, a quadratic nonlinearity (i.e. a system response $\propto P^2$) will generate harmonics at $2\omega_p$; higher order nonlinearities give commensurate harmonics ($3\omega_p$ etc. though if the received signal is 'clipped', i.e. detector is saturated, odd harmonic peaks will be artificially enhanced). This has been used to detect bubbles of specific size, resonant at 0.89 MHz in one experiment [19] and at both this and at 1.64 MHz in another [20]. If such systems are to be perfect bubble detectors then the condition must hold that only resonant bubbles can generate the required nonlinearity, and in the presence of only non-resonant bubbles, ω_p alone is detected. However whilst the emission of the second harmonic is a global maximum at resonance, the $2\omega_p$ signal can arise through non-bubble sources of nonlinearity, which must be carefully examined. Such sources do not include solid inhomogeneities. The same condition holds if the applied field contains two frequencies, i.e. $P=A\cos\omega_p t + B\cos\omega_i t$ where $\omega_p << \omega_i$. The 'imaging' frequency (ω_i) scatters geometrically from a target (the pulsating bubble) whose cross-sectional area varies periodically [9]. The detected signal consists of ω_i, modulated at frequency ω_p, and the resulting detection of $\omega_i \pm \omega_p$ in the received spectrum has been used to size a bubble spectrum by employing the assumption that, bar the presence of resonant bubbles, only ω_i and ω_p are detected [8,21]. The assumption fails if the pulsation of non-resonant bubbles, or the presence of a quadratic nonlinearity anywhere in the system, is sufficient to generate $\omega_i \pm \omega_p$. One advantage of combination-frequency methods is that the bubble resonance generates a signal in the MHz range (close to ω_i), removing it from 'masking' signals such as the acoustic input and ambient noise.

All the above techniques for bubble sizing which exploit the bubble resonance suffer in that sources other than resonant bubbles (e.g. turbulence, transducer effects etc.) can to a greater or lesser extent generate the desired signal, indicating the presence of a resonant bubble when one is not present [4]. Such 'false triggering' has not to date been found when signals at $\omega_i \pm \omega_p/2$, generated when the amplitude component A of the insonating field $P=A\cos\omega_p t + B\cos\omega_i t$ exceeds the threshold value required to generate Faraday waves on the bubble surface, are used for bubble sizing [9]. Characteristics of the acoustic sizing various techniques are summarised in Table 1.

Scatters	**Advantage**	**Disadvantage**	**Prior application**	**Bubble sizes investigated in a single expt.**
Geometric	Rapidly obtains images with high spatial (location) resolution	Cannot distinguish between bubbles and solid particles	Laboratory [16,18,23]	Distribution (low radius resolution)
Funda-mental	Apparatus simple	Large bubbles and bubble clouds may falsely register as resonant bubble (geometric scattering). Low spatial resolution. False triggering and off-resonance scattering may occur. High number densities only are valid if 'bulk properties' are assigned to the liquid.	Resonator [22] Attenuation [6] Backscatter [14]	Four [13]; around nine [7, 22]
Second harmonic	Little contribution from geometric scattering.	Low spatial resolution. False triggering and off-resonance scattering may occur.	Clinical, detecting ≈μm radius bubbles [19,20]]	One [19] or two [20] per trial
$\omega_i \pm \omega_p$	No threshold.	False triggering and off-resonance scattering may occur.	Lab. [8,21], field [24]	Distribution
$\omega_i \pm \omega_p/2$	Minimal false triggering or, at threshold, off-resonance scattering.	Insonation at the threshold acoustic pressure is required for fine radius resolution.	Laboratory [9,25-27]	One @ 25 Hz resolution [9]

Table 1: The various acoustic techniques available for bubble detection. Numerals in columns 5 and 6 are references.

The less prone a system is to 'false triggering', the more complicated in general it is to deploy. It therefore would be desirable to be able to deploy a range of these techniques to interrogate a given liquid sample, either sequentially or concurrently as defined by the problem. This would enable optimisation of the process of characterising the bubble population in the liquid with respect to minimising the ambiguity of the result and the complexity of the task. The task itself involves first the detection of inhomogeneities in liquids. In certain circumstances it is then necessary to analyse the sample further to distinguish gas bubbles from solid or immiscible liquid-phase inclusions. The final stage of analysis would involve not only the detection, but also the sizing of the gas inclusions, leading to the characterisation of the bubble population. This can be summarised in a four-part *Ideal objective* [28]: (i) Detect

MULTIPLE ACOUSTIC TECHNIQUES FOR BUBBLE DETECTION

inhomogeneities in liquids; (ii) Distinguish gas bubbles from solids; (iii) Measure radii of bubbles present; (iv) Measure number of bubbles in each radius class.

This study introduces a method by which the *ideal objective* might eventually be achieved, using a range of techniques. The limitations of each can be compensated through the deployment of others. Since the ambiguities of each have been studied theoretically and experimentally [15], the initial emphasis of this study will be how successfully each technique can provide information about simple controlled populations (stationary single and paired bubbles). Rising bubble streams will then be measured. The techniques listed in Table 1 are used, so that bubble detection is achieved through the geometric scattering of 3.5 MHz ultrasound (using a scanner in both B and M modes simultaneously), and through scattering of signals at ω_p, $2\omega_p$, $\omega_p/2$, $\omega_i \pm \omega_p$, $\omega_i \pm 2\omega_p$, $\omega_i \pm \omega_p/2$ and $\omega_i \pm 3\omega_p/2$. This is done for broadband, and increasing, incremented, tonal 'pump' signals.

3. METHOD

There exist detection zones, at 15 cm depth, for the various active acoustic sizing systems detection (including those listed in Table 1), comprising the overlap of beam patterns of relevant transducers held in rigid 'cage' configuration (Figure 1). The cage is placed at depth 0.15 m in a 1.8 m x 1.2 m x 1.2 m deep vibration isolated glass reinforced plastic tank. The bubble population is either injected into the tank below these zones, and then rise to pass through them, or consists of two bubbles attached to a wire, held within the intersection of the zones. The required 'pump' signal (which drives the bubbles into oscillation), be it broadband, or a series of tones $P=A\cos\omega_p t$ where ω_p is incremented in 50 Hz (tethered bubbles) or 100 Hz (moving bubbles) steps, is generated by a Gearing and Watson UW60 loudspeaker (having a frequency response flat to within ±5 dB over the range 500 Hz -10 kHz). During combination-frequency tests the imaging signal $P= B\cos\omega_i t$ is generated by a Therasonic 1030 (Electro-Medical Supplies) fixed at 1.134 MHz, and a Panametrics V302 receiver detects the MHz signal before it is heterodyned with the Therasonic signal. The Bruel and Kjaer 8103 hydrophone ('HP1') is used to detect signals not involving combination frequencies. The heterodyned high-frequency signal and the B&K 8103 signals are acquired to the PC via a GPIB-controlled Digital Storage Oscilloscope (LeCroy 9314L). Calibration is made with no bubbles present to allow compensation of the acoustic response of the water, apparatus, and tank. This enables the sample to be insonated at equal amplitudes when interrogated by a sequence of tonal pumping signals, each of 0.2 s duration. Data is only collected after a 'start-up' time of the first 7.5 ms for tethered bubbles, to allow transients to die away; no such delay can be afforded with rapidly-rising, mm-sized bubbles, though averaging over the 10^4 samples of each increment reduces the transient effect. Including data collection, increments start 1.6 s apart.

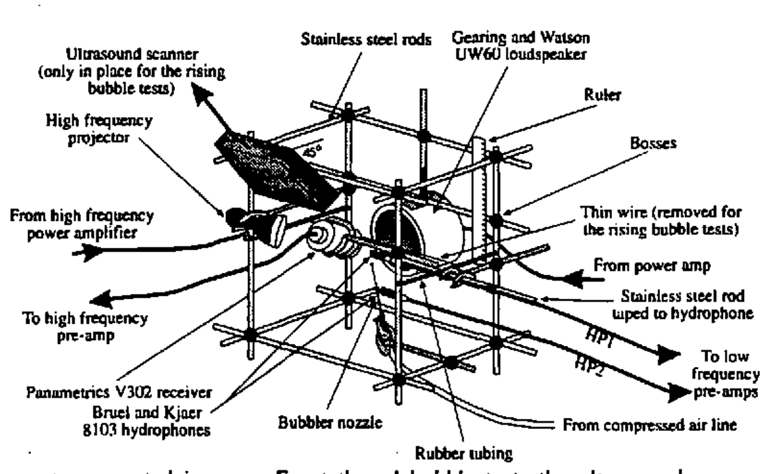

Fig. 1. Schematic of apparatus mounted in cage. For tethered bubble tests the ultrasound scanner is removed. For rising bubble tests the thin wire in cage centre is removed.

MULTIPLE ACOUSTIC TECHNIQUES FOR BUBBLE DETECTION

The rising bubbles are injected from a needle attached to a compressed air-line. The passive acoustic signal so generated in detected by 'HP2', a hydrophone (Bruel and Kjaer 8103) 10 mm from the needle tip (depth, 29 cm). This is analysed for exponentially-decaying sinusoid 'signatures' for the generation of each bubble, the frequency of the sinusoid indicating the bubble size. However with higher entrainment rates (where signatures overlap) in noisy environments, individual entrainments may not be detected even in time-frequency representation (TFR), where resolution in time and frequency is a compromise determined by the size of the window imposed upon the data. However a TFR of the Gabor coefficients, rather than the acoustic power invested in each frequency band, will readily identify the bubble signatures [29-31]. A routine thresholds on the value and gradient of the Gabor coefficients, then automatically counts and sizes the bubbles, giving their rate of production before they rise into the active detection zones. A second count is made by placing a greased Petri dish in the rising bubble stream above the detection zones. Photographic measurement of the bubbles adhering to the thin layer of silicone grease were taken. However compensation must be made in comparing the bubble population measured in given volumes of liquid by the active techniques, with the captured population on the dish and the rate of bubble generation measured at the needle by the Gabor technique, since for example the volume of the bubble stream sampled by the Petri dish is greater the greater the bubble rise speed. The volume changes caused by the varying hydrostatic pressure are accounted for in comparing all measurements. The sizes of the two bubbles attached to the wire were checked by detaching them from the wire into small glass flasks, in which they were transferred to a travelling microscope for measurement [25].

A Hitachi EUB-26E 3.5 MHz ultrasound scanner, mounted in the cage, gave M- and B-mode images of the rising bubbles. Atmospheric pressure was 0.1003 MPa.

Detection through scattering at ω_p and $\omega_i \pm \omega_p$ require only linear bubble pulsations, so that the relatively low energy densities per frequency band afforded by broadband insonation (band limited white noise between 1000-8000 Hz) is appropriate. This rapidly allows an estimate of the region wherein the bubble resonances lie, for later application of the nonlinear detection signals ($2\omega_p$, $\omega_p/2$, $\omega_i \pm \omega_p/2$, $\omega_i \pm 2\omega_p$, $\omega_i \pm 3\omega_p/2$) which require an incremented pure tone pump signal necessary (i) to drive at high enough amplitude; and (ii) because the detector frequency emitted by a bubble differs from that which drives it at resonance, which would cause ambiguity if broadband excitation were employed.

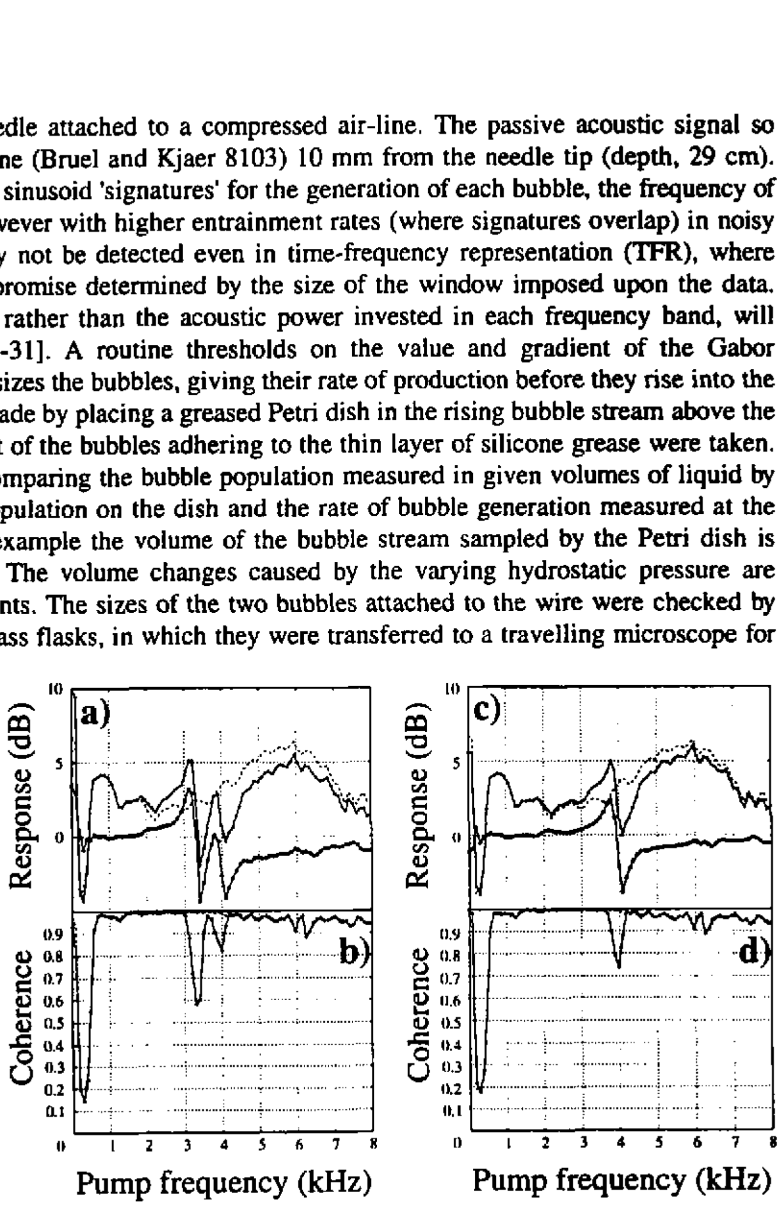

Fig. 2 Response (modulus of voltage transfer function, plots 'a' and 'c') and coherence ('b' and 'd') for broadband insonation (band limited 1-8 kHz) of both ('a' and 'b') tethered bubbles, and for just the smaller ('c' and 'd'): dashed line = 'in absence of bubbles'; –+–+– = 'in presence of bubbles'; —●—●— = ratio of 'bubble present' to 'bubbles absent' signals. Resolution: 98 Hz.

4. RESULTS

4.1 Two tethered bubbles

The first of the results are shown in Fig. 2 for the broadband excitation of two bubbles attached to a wire 10 mm apart. Throughout the paper a dashed line indicates signal with no bubbles present; a solid line with crosses indicates the signal in presence of bubble(s); and a thick solid line with closed circles indicates the ratio of the signal 'with' bubbles to that 'without' bubbles, i.e. the bubble-mediated amplification. Data points occur at symbols, and at equivalent frequencies for dashed lines. Fig. 2a illustrates the difference in the modulus of the voltage transfer function (the ratio of output to input) when the bubbles were driven by band-limited (1-8 kHz) white noise. The response shows peaks at 3.1 and 3.9 kHz (±0.1 kHz), with a sharp dip ~300 Hz above each. This reflects the through - resonance behaviour of each bubble: at frequencies just below resonance the sound field and the bubble pulsations (which scatter significantly more than they do away from resonance) are in phase and constructively interfere, but above resonance the bubble undergoes a π phase shift such that it now pulsates in antiphase with the driving sound field, resulting in destructive interference. This behaviour suggests that the change in signal which results from bubble presence does not represent geometric scattering from a large bubble or other body, but is due to the presence of resonant bubbles in that frequency range. Even several kHz above the resonance of the pair, the detected signal is ~1 dB less than the levels at low frequencies, and those found in the absence of bubbles, as a result of the destructive interference caused by the whole population, and it may be that this can be used to characterise a population (compare this reduction with the smaller one seen in Fig. 2c for one of these bubbles on its own). The coherence between the signal input to the source and the returned signal (Fig. 2b) shows a definite bubble-mediated reduction in the signal around 3.3±0.15 and 4±0.15 kHz. As these coherence dips appear at frequencies mid-way between the peaks and troughs

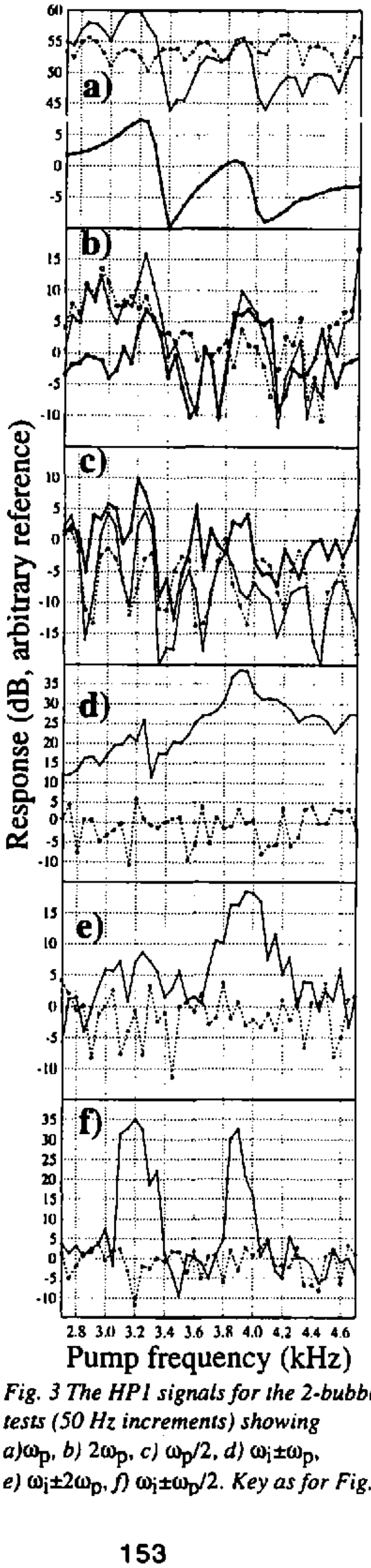

Fig. 3 The HP1 signals for the 2-bubble tests (50 Hz increments) showing a)ω_p, b) $2\omega_p$, c) $\omega_p/2$, d) $\omega_i \pm \omega_p$, e) $\omega_i \pm 2\omega_p$, f) $\omega_i \pm \omega_p/2$. Key as for Fig. 4.

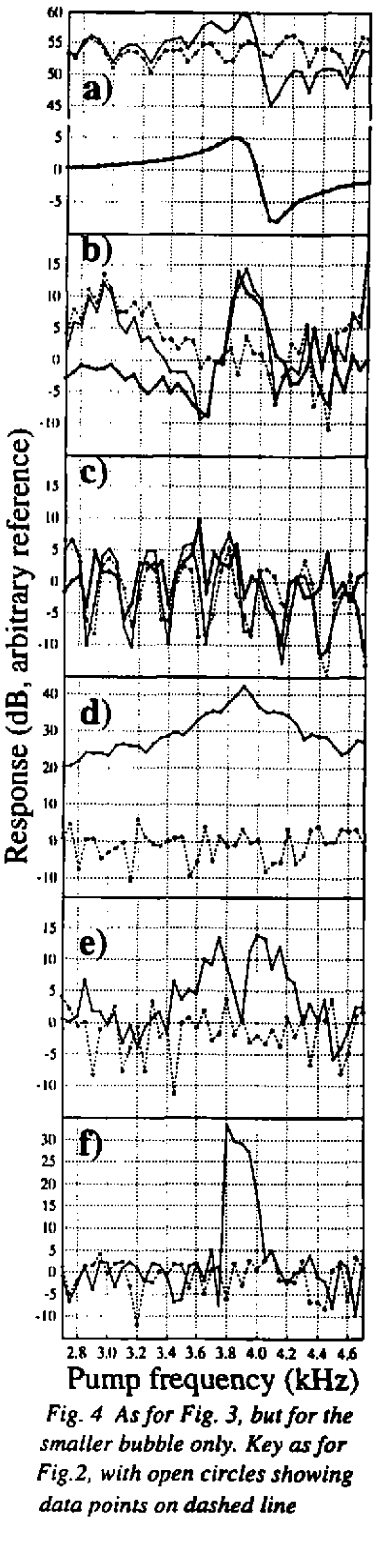

Fig. 4 As for Fig. 3, but for the smaller bubble only. Key as for Fig.2, with open circles showing data points on dashed line

in the transfer function (Fig. 2a) they appear to indicate a bubble nonlinearity rather than a reduced signal to noise ratio, which would be the case if the dips in Figs. 2a and 2b occurred at the same frequency.

Figs. 2c and 2d show the transfer function and coherence resulting from broadband excitation when the bubble resonant at ~3.3 kHz is removed after completion of the two-bubble tests. The other peak remains at 3.9±0.1 kHz, suggesting that to within this resolution the bubbles were far enough apart (approximately 10 bubble radii) for the bigger bubble not to significantly influence the resonance frequency of the other [32]. The peak is about 3 dB higher than in the two bubble test even though the same excitation amplitude was used. This is due to the removal of the antiphase bubble pulsation of the larger bubble beyond its resonance which therefore means that there is no destructively interfering component on the smaller bubble's pulsation below its resonance. The coherence again shows a similar dip to the relevant one found in the two bubble test.

Having through 1 s (5 averages) of broadband insonation of the two bubbles reduced the range of interest for further investigation from 1-8 kHz to be 2.7-4.7 kHz, the bubble pair was excited (with pump amplitude 120 Pa (0-pk)) at 40 discrete increasing frequencies in 50 Hz increments: At 1.6 s per increment, the test took 64 s. The results are given in Fig. 3 for the harmonic (parts a-c) and sum-and-difference (parts d-f) signals, monitored simultaneously. The data is displayed as the magnitude in the frequency spectra of the signal of interest (i.e. ω_p, $2\omega_p$, $\omega_p/2$, $\omega_i \pm \omega_p$, $\omega_i \pm 2\omega_p$ and $\omega_i \pm \omega_p/2$) corresponding to each pump frequency. The data was sampled at 50 kHz, and the FFT frequency resolution with 8192 points was 6 Hz. The test was repeated following the removal of the larger bubble (Fig. 4).

The fundamental backscatter (Fig. 3a) shows a rippled amplitude response in the absence of a bubble, which is due to the differences in the proximity of each pumping signal tone to a FFT bin centre frequency. This effect disappears when the dB difference ('amplification') between the signal with, and without, bubbles is taken, revealing again the characteristic through-resonance response indicating the presence of resonant bubbles at 3325±70 and 3900±100 Hz. The response of the second harmonic (Fig. 3b) is less clear. The height of the signal in the absence of the bubble can be affected for instance by the relative levels of harmonic distortion in the equipment and also the proximity of the signal to a frequency bin. Nevertheless, there still appears to be a clear increase in the signal between 3200-3400 Hz and 3800-4100 Hz. Removal of the larger bubble has negligible effect in the peaks in the first harmonic and second harmonic response for the smaller bubble as shown in Figs. 4a and 4b. The emissions of $\omega_p/2$ from both two bubbles (Fig. 3c) and the smaller one (Fig. 4c) are confused by numerous spurious peaks. The amplitude of the heterodyned

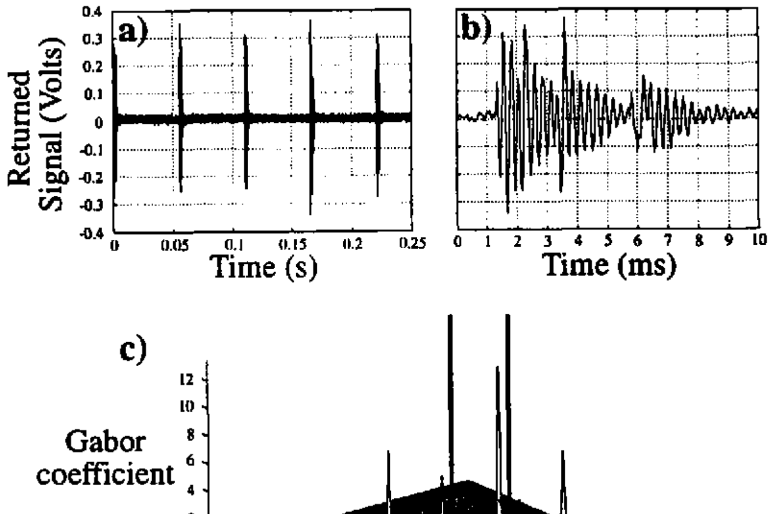

Fig. 5 The HP2 signal during injection. a) Time series (detail shown in 'b'). c) Time-frequency representation of Gabor coeffs. associated with 'a' (first peak removed for clarity). Where multiple coeffs are identified with injection of a single bubble, the later one (arrowed) gives natural frequency.

MULTIPLE ACOUSTIC TECHNIQUES FOR BUBBLE DETECTION

returned signal from the high frequency receiver at $\omega_i \pm \omega_p$, $\omega_i \pm 2\omega_p$ and $\omega_i \pm \omega_p/2$ are shown in Fig. 3d-f as a function of the incrementing pumping frequency ω_p. Though there maxima at 3.25±0.05 and 3.9±0.2 kHz, the signal at $\omega_i \pm \omega_p$ (Fig. 3d) is present at more than 12 dB above the "no bubble" signal over the entire pumping frequency range. Clearly, the off-resonance contribution to the returned signal limits the resolution of the measurement for the bubble's resonance frequency. Though the off-resonance contribution is less for $\omega_i \pm 2\omega_p$ (Fig. 3e) the resolution of the high-frequency peak is similarly poor (4±0.2 kHz), and there are spurious maxima. The $\omega_i \pm \omega_p/2$ (Fig. 3f) best shows the presence of two bubbles, resonating at 3.2±0.1 and 3.88±0.05 kHz. The off-resonance contributions are negligible. Removal of the larger bubble demonstrates the same features in the detection of the remaining bubble (Fig. 4) by the d) $\omega_i \pm \omega_p$, e) $\omega_i \pm 2\omega_p$ and f) $\omega_i \pm \omega_p/2$ signals.

4.2 Injected bubbles

Fig. 5 shows a portion of the bubble stream as measured through the passive acoustic emissions generated on injection. In Fig. 5a, a 0.25 s section of the time series recorded by the hydrophone HP2 indicates individual bubbles being repeatably generated every ~0.06 s. Each of the bubble signatures has the form, not of a single exponentially-decaying transient, but of multiple ones, revealing that the released bubble is excited on three subsequent occasions following the initial release from the needle (Fig. 5b). These excitations arise through contact, and usually coalescence, between the newly-released bubble and the successor gas pocket growing at the nozzle tip [33]. As a result the plot of the Gabor coefficients (Fig. 5c) may reveal multiple peaks for a single bubble (which vary each time, showing the nozzle process is not entirely repeatable). Clearly the frequency at which the final peak of each group occurs (arrowed in Fig. 5c) is the one which relates to the size of the final bubble after it has escaped clear of the contact/coalescent processes that occur at the nozzle, and it is this size which is taken to be measure of the bubble size upon injection.

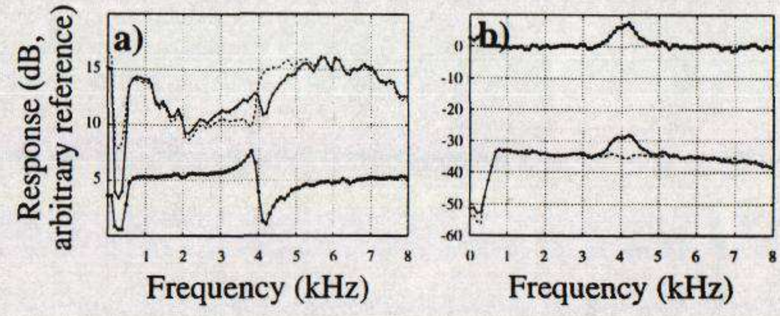

Fig. 6 Response (modulus of voltage transfer) for broadband insonation (band limited 1-8 kHz) of rising bubbles, from a) HP1, and b) heterodyned high-frequency (from V302), signals. Resolution: 98 Hz. Key as for Fig 2.

In Fig. 6 the results of broadband insonation in the frequency range 1 to 8 kHz is shown. In Fig. 6a, the signal picked up by HP1 is shown, both for the situation before the bubble stream began, and for the scattered signal in the presence of the bubble stream. The difference between the two signals is plotted, showing significant changes in the frequency range 3.5 to 5 kHz, indicating the through-resonance effect described above, centred around 4±0.1 kHz. In Fig. 6b, the heterodyned signal from the high frequency receiver transducer shows bubble-mediated change from 3.5 to 4.9 kHz (centred at 4.2±0.3 kHz). An 800 Hz high pass filter was placed after the heterodyning so that the strong Doppler components of the returned signal did not overload the input channel to the oscilloscope.

Having rapidly found the region of interest (3.3 to 4.3 kHz) through the broadband technique, the pump sound field is incremented in this range in steps of 100 Hz, at a pressure amplitude of 240 Pa (0-pk). Fig. 7 shows the results of analysis of the signal recorded by hydrophone HP1. In Fig. 7a, the scattering of the fundamental frequency ω_p gives f_0≈3850±20 Hz. The second harmonic $2\omega_p$ neither immediately indicates a distribution around a single bubble size (Fig. 7b), nor accurately what that size might be (f_0≈3.8±0.15 kHz), suggesting in fact a bimodal distribution. The $\omega_p/2$ results are similarly unclear (Fig. 3c). During the same single pass from 3.2 to 4.4 kHz as was made for Fig. 7 were taken the results for Fig. 8, a histogram showing the received, heterodyned spectrum as a function of the pump frequency (this, on the horizontal axis, indicating not a continuum but the 12 settings of the pump frequency, since the latter was incremented in 100 Hz steps).

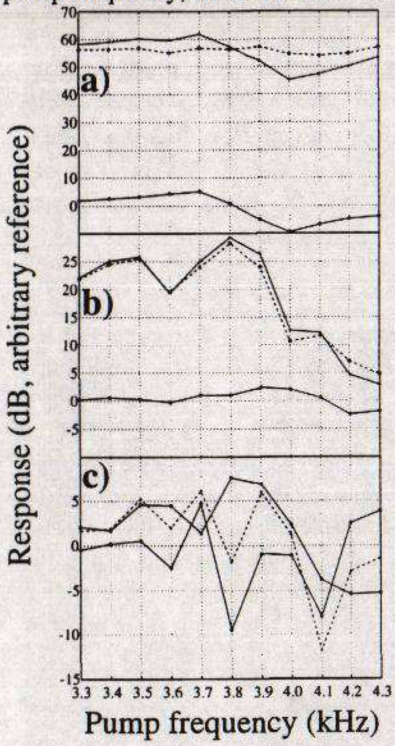

Fig. 7 Response at a) ω_p, b) $2\omega_p$, c) $\omega_p/2$ in the HP1 signal for insonation in 100 Hz increments. Key as for Fig. 4.

In the greyscale plot, signals at $\omega_i \pm \omega_p$, $\omega_i \pm 2\omega_p$ and $\omega_i \pm \omega_p/2$ are labelled. It is not possible to determine the size of bubbles using the $\omega_i \pm \omega_p$ plot, which suggests a broad range of sizes are present over more than a kHz range.

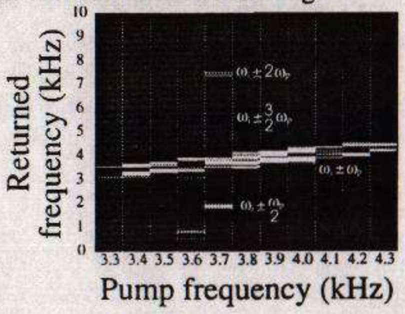

Fig. 8 Greyscale histogram showing heterodyned received signal (from V302) for each discrete setting of the pump frequency (100 Hz increments). Light shades indicate strong signal. Signals at $\omega_i \pm \omega_p/2$, $\omega_i \pm \omega_p$, $\omega_i \pm 3\omega_p/2$ and $\omega_i \pm 2\omega_p$ are indicated.

The clearest indication of resonance is that only for the pump frequency setting of 3.7 kHz does structure in the heterodyned spectrum at frequencies which are multiples of $\omega_p/2$ (corresponding to $\omega_p/2$, ω_p, $3\omega_p/2$, and $2\omega_p$) occur. All other peaks do not correspond to multiples of ω_p. Fig. 9 shows both the a) M- and b) B-mode images obtained using the Hitachi ultrasound scanner, the section shown being a slice at 45° to vertical (Fig 1). The bubble (labelled B) can be located in Fig. 9b (near-field is at top of image), which also images the loudspeaker (S) and part of the cage. The images which intersect the vertical line (L) in 1 s are plotted in Fig. 9a: almost 19 bubbles pass through the beam in that time, with rise speed (from the image, within the limits of the rectilinear bubble motion, adjusting for the 45° orientation) of 20±2 cm/s. Comparison of 'a' with 'b' allows the transient features (e.g. bubbles) to be distinguished from the time-invariant ones (e.g. cage and speaker).

5. DISCUSSION

← Broadband pump signal → ← Pump signal incremented in 50 Hz steps (frequency increasing) →

	Amplitude ω_p	Coherence ω_p	ω_p	$2\omega_p$	$\omega_p/2$	$\omega_i \pm \omega_p$	$\omega_i \pm 2\omega_p$	$\omega_i \pm \omega_p/2$
Distribution indicated	(2a) Two bubbles	(2b) Two bubbles	(3a) Two bubbles	Spurious peaks (3b)	Spurious peaks (3c)	(3d) Two bubbles	Unclear peaks (3e)	(3f) Two bubbles
Resonance freq. f_0 /kHz	3.3±0.1 4.0±0.2	3.3±0.15 4.0±0.15	3.33±0.07 3.9±0.1	3.3±0.1 3.95±0.15	3.2±0.1 -	3.25±0.05 3.9±0.2	- 4±0.2	3.2±0.1 3.88±0.05
$\frac{R_0}{\mu m} \approx \frac{p_0^{1/2}}{100 f_0}$	970±30 800±40	970±44 800±30	960±20 820±20	970±30 810±30	1000±30 -	980±15 820±42	- 800±40	1000±30 820±10

Table 2. Resonances and calculated radii of the two tethered bubbles. (p_0=101770 Pa). References in row 2 are to figs.

For the two tethered bubbles, optical measurements gave radius estimates of 1.1±0.1 and 0.8±0.1 mm. Fig. 3f most clearly indicates the presence of two bubbles is, plotting $\omega_i \pm \omega_p/2$. Table 2 summarises the information gleaned from each signal type in the two-bubble test. Though no high-resolution technique determines both resonances to the same accuracy, the best overall resolution is obtained from $\omega_i \pm \omega_p/2$ using incremented pump signals. Initial use of broadband first reduced the test time by a factor of 64. Unlike the other techniques, the resolution of $\omega_i \pm \omega_p/2$ can be dramatically affected by the acoustic pressure at the bubble: whilst it could be improved to ±12 Hz by insonating at the threshold pressure [9], there is no guarantee that in the general case this threshold can be accurately delivered.

This is particularly true when considering the results from moving bubbles (Table 3), since each bubble is transitory. Also because of this, not only the accuracy but also the population sampling must be considered. In fact, the results in Table 3 refer to two quite separate populations. First the incremented techniques (whilst they can be repeated to average a steady-state population [9]) were here in fact applied in one pass, and so would ideally detect signals only from resonant bubbles which are in the detection zone during the 0.2 s of each tone. Since bubbles are generated at ~60 ms intervals, and have a rise time of 20±2 cm/s, all the incremented tests (columns 4-10) sample in each increment the same population of ~4 bubbles (different sets of ~4 bubbles for each of the 40 increments - 'population 1'). Three mins. later the broadband techniques sample across the entire frequency range for five 0.2 s averages, totalling 1 s: The results in cols. 2 and 3 therefore sample a population of ~19 bubbles ('population 2'). Though there are differences in resolution between the broadband and the incremented techniques, the results in Table 3 indicate that the two populations differed, the one measured first having a lower resonance (3.7±0.05 kHz) that the other (4±0.1 kHz). This issue will be discussed later.

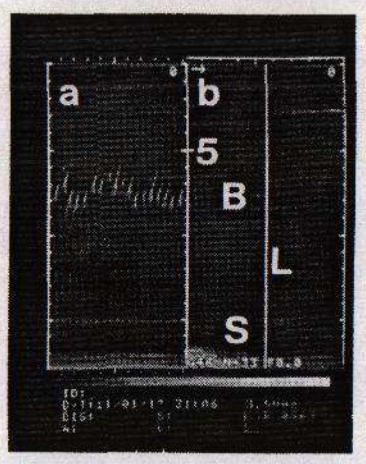

Fig. 9 a) M-mode (1 s sweep) and b) B-mode images from Hitachi ultrasound scanner. In 'b' a bubble (B), UW60 speaker (S), the 5 cm marker from transducer faceplate (at top of image) and the line (L, occurrence of an image in which defines the M-mode image) are indicated.

Resolution of the ω_p and $\omega_i \pm \omega_p$ signals is roughly constant between broadband and incremented forcing at around 100 Hz and 300-500 Hz respectively (Table 3). The ω_p signal is not pronounced and would readily be confused by a wide range of sizes (see Table 2). The resonance is indicated not by the maximum (strong emission almost in phase with driver), but by the in-phase point *between* the maximum and the minimum (antiphase) point: this has implications for studies where the scattering is assumed to be from resonant bubbles only. Only the simultaneous occurrence of the structure at $\omega_i \pm \omega_p/2$, $\omega_i \pm 3\omega_p/2$, and $\omega_i \pm 2\omega_p$ allows accurate active characterisation. It is not surprising that the $\omega_i \pm \omega_p/2$ signal should so clearly indicate the resonance, whereas the $\omega_p/2$ signal does not, since only the former can exploit the imaging beam to propagate to distance.

← Broadband → ←—— Incremented pump, 100 Hz steps, frequency increasing ——→

POPULATION 2 ←—————— POPULATION 1 ——————→

Column 1	Column 2	Column 3	Column 4	Column 5	Column 6	Column 7	Column 8	Column 9	Column 10
Signal:	ω_p	$\omega_i \pm \omega_p$	ω_p	$2\omega_p$	$\omega_p/2$	$\omega_i \pm \omega_p$	$\omega_i \pm \omega_p/2$	$\omega_i \pm 2\omega_p$	$\omega_i \pm 3\omega_p/2$
Distribution indicated	Narrow (Fig 6a)	Broad (Fig 6b)	Narrow (Fig 7a)	Bimodal (Fig 7b)	Bimodal (Fig 7c)	Broad (Fig 8)	Narrow (Fig 8)	Narrow (Fig 8)	Narrow (Fig 8)
Resonance freq. f_0 /kHz	4 ±0.1	4.2 ±0.3	3.85 ±0.1	3.8 ±0.15	3.9 ±0.2	3.8 ±0.5	3.7 ±0.05	3.7 ±0.05	3.7 ±0.05
$\frac{R_0}{\mu m} \approx \frac{p_0^{1/2}}{100 f_0}$	800 ±20	760 ±50	830 ±22	840 ±33	820 ±42	840 ±110	862 ±12	862 ±12	862 ±12

Table 3. Resonances and calculated radii of rising bubbles for populations 2 (broadband pump) and 1 (incremented pump).

The question of whether the two populations, measured by broadband and incremented techniques, could possess the distribution difference suggested above must be addressed by reference to the other techniques used for determining the bubble size some minutes after the conclusion of the broadband tests. The ±2 cm/s standard deviation on the 20 cm/s rise time translates to estimated lower and upper limits for radius in clean water of 0.87

and 1.13 mm [34]. Clearly this is not sufficiently discerning. The distribution of rising bubbles from four Petri dish photographs (taken 10 minutes after the end of the passive Gabor tests and corrected for hydrostatic head) gives for the size @ 15 cm depth: 790±60 μm (28 bubbles collected in 1.5 s); 790±120 μm (24 bubbles in 1.3 s); 830±80 μm (27 bubbles in 1.4 s); 820±130 μm (32 bubbles in 1.7 s). There is some indication of occasional larger bubbles in a more uniform distribution.

Trial	Test 1	Test 2	Test 3
Natural freq-uencies /Hz	3722 3737 3190 3550 3736	3751 3699 3642 3758 3835	4018 4015 3219 3965 4021
Average freq./Hz	3580 ±240	3740 ±70	3850 ±350
R_0 /μ m @ 29 cm	897 ±60	859 ±15	834 ±76
R_0 /μ m @ 15 cm	901 ±60	863 ±16	838 ±75

Table 4. Natural freqs. & calculated average radii from Gabor tests @ 29 & 15 cm depths.

The actual stability of the population is best determined by the Gabor tests. Three of these were performed at one minute intervals after the broadband tests, and before the ultrasonic images, were taken. In each test 0.25 s of passive emissions, comprising the injection emissions of five consecutive bubbles, were taken (Fig. 5a represents test 2). The natural frequencies so found are shown in Table 4, with the average for each test, and the calculated bubble size distribution at the needle (29 cm depth) and at the zone of the active detector (15 cm depth). Clearly, variation in the size of the generated bubbles can occur. This is not unexepected when compressed air, supplied from a line, is bubbled at rates high enough for inter-bubble contact/coalescence to occur. Table 4 suggests that the variation found during the 1 s of the broadband test, and the 40x1.6 s of the incremented test, is of the same order as the standard deviations quoted in Table 3. Clearly for all but the technique with the highest resolution in each population, the standard deviation represents the resolution limitations of the techniques. The fact that for the highest resolution (cols. 8-10 for population 1; col. 2 for population 2) the uncertainties in Table 3 are similar to those quoted for these techniques during the two-bubble test (Table 2), when the population was stable, suggests that the standard deviations reflect limits in resolution. It seems that in fact the best resolution limits in each case are very similar to the variability one might expect in the population. Though by no way conclusive, it is suggestive that the large standard deviations in tests 1 and 3 result from single freak values. These values could well escape detection in the 0.2 s duration of each incremented tone, and if the item 3190 Hz is removed from test 1 the average becomes 3686±90 Hz (871±21 and 875±21 μm @ 29 and 15 cm depth respectively); and if the item 3219 Hz is eliminated from test 3, the average becomes 4004±30 Hz (giving 802±6 and 806±6 μm @ 29 and 15 cm depth respectively). This variation is less than the resolution limits of Table 2, and the uncertainties quoted in Table 3, for the $\omega_i \pm \omega_p/2$ and related tests.

Without doubt the Gabor technique is not only the most simple and accurate but also samples the entire population, being capable of logging the natural frequency of each and every bubble that is generated in near real-time to 1 Hz accuracy (even giving details of nozzle processes). However the Gabor signal must be interpreted carefully. Firstly, it reflects the natural frequency of a damped system, given by $\omega_0(1-\delta^2)$, where δ is the dimensionless damping coefficient [35] and ω_0 the undamped natural frequency: active techniques in general measure the maximum of the amplitude response, which occurs at frequency $\omega_0(1-2\delta^2)$. The two major limitations are, first that the signal becomes increasingly difficult to interpret as the entrainment rate increases. Second, passive emissions usually give information only about the bubbles being entrained at that moment, the excitation that is strong enough to make adequate emissions usually requiring the closure of a liquid surface [15]: Older, 'silent' bubbles would have to be excited by impulse to ring, and a sufficiently strong impulse would alter the bubble population by inducing more closures (i.e. fragmentation).

MULTIPLE ACOUSTIC TECHNIQUES FOR BUBBLE DETECTION

4. CONCLUSIONS

Broadband insonation rapidly indicates the range over which bubble resonances may occur, reducing the time required for tonal incrementation. Best resolution and population sampling was achieved using the Gabor technique, though this operates only on entrainment. The best active indicator of the bubble population was the $\omega_i \pm \omega_p/2$ signal, though it must be remembered that this signal is not simple to implement: For best resolution the acoustic pressure amplitude at the bubble must be close to the threshold [9], and a delay after insonation at a given frequency commences is recommended, to allow the transients to decay before data is acquired .

Acknowledgements Our thanks to EPSRC (ref. GR/H 79815) for funding, and to PR White for advice.

REFERENCES

[1] DETSCH RM & SHARMA RN. The critical angle for gas bubble entrainment by plunging liquid jets. *Chemical Engineering J* (1990) 157-66.

[2] TICKNER EG. Precision microbubbles for right side intercardiac pressure and flow measurements. In: *Contrast Echocardiography, Meltzer, R. S., Roeland, J. (eds.)*, (Nijhoff, London) (1982)

[3] WOOLF DK. Bubbles and the air-sea transfer velocity of gases. *Atmos.-Ocean* (1993) **31** 451-474

[4] LEIGHTON TG. Acoustic Bubble Detection. I. The detection of stable gas bodies *Environmental Engineering* (1994) **7** 9-16

[5] LEIGHTON TG. Acoustic Bubble Detection. II. The detection of transient cavitation. *Environmental Engineering* (1995) **8** 16-25

[6] MEDWIN H. In situ acoustic measurements of microbubbles at sea. *J Geophys Res* (1977) **82** 971-976

[7] MEDWIN H & BREITZ ND. Ambient and transient bubble spectral densities in quiescent seas and under spilling breakers. *J Geophys Res* (1989) **94**12751-12759

[8] NEWHOUSE VL & SHANKAR PM. Bubble size measurement using the nonlinear mixing of two frequencies. *JASA*. (1984) **75** 1473-1477

[9] PHELPS AD & LEIGHTON TG. High resolution bubble sizing through detection of the subharmonic response with a two frequency excitation technique. *J. Acoust. Soc. Am.* (1995) In press.

[10] NISHI RY. Ultrasonic detection of bubbles with Doppler flow transducers. *Ultrasonics* (1972) **10** 173-179

[11] STRASBERG M. Gas bubbles as sources of sound in water, *J.Acoust.Soc.Am.* (1956) **28** 20-26

[12] LEIGHTON TG & WALTON AJ. An experimental study of the sound emitted from gas bubbles in a liquid. *Eur. J. Phys.*(19870 **8** 98-104

[13] FARMER DM & VAGLE S. Waveguide propagation of ambient sound in the ocean-surface bubble layer. *JASA*. (1989) **86** 1897-1908

[14] THORPE SA. Measurements with an Automatically Recording Inverted Echo Sounder; ARIES and the Bubble Clouds. *Journal of Physical Oceanography* (1986) **16** 1462-1478

[15] LEIGHTON TG. The Acoustic Bubble *Academic Press, London.* (1994) 234-243; 295-298; 439-464

[16] MORRISS SL & HILL AD. Ultrasonic imaging and velocimetry in two-phase pipe flow. *Trans. ASME* (1993) **115** 108-116

[17] VAN DER WELLE R. Void fraction, bubble velocity and bubble size in two phase flow. *Int. J. Multiphase Flow* (1985) **11** 317-45

[18] KOLBE WF, TURKO BT & LESKOVAR B. Fast ultrasonic imaging in a liquid filled pipe. *IEEE Trans. Nucl. Sci.* (1986) **33** 715-722

[19] MILLER DL Ultrasonic detection of resonant cavitation bubbles in a flow tube by their second harmonic emissions. *Ultrasonics*(1981) **19** 217-24

[20] MILLER DL, WILLIAMS AR & GROSS DR. Characterisation of cavitation in a flow-through exposure chamber by means of a resonant bubble detector. *Ultrasonics* (1984) **22** 224-230

[21] SCHMITT RM, SCHMITT HJ & SIEGERT J. *In vitro* estimation of bubble diameter distribution with ultrasound. *IEEE Eng in Med and Biol Soc* (1987) 9th Ann Conf 13-6

[22] BREITZ N, MEDWIN H. Instrumentation for in-situ acoustical measurements of bubble spectra under breaking waves *JASA*(1989) **86** 739-43

[23] BLACKLEDGE JM. B-scan imaging of two phase flows. IEE Colloquium on 'Ultrasound in the process industry', p5/1-17 Sept. 23rd 1993

[24] KOLLER D, LI Y, SHANKAR PM & NEWHOUSE VL. High-speed bubble sizing using the double frequency technique for oceanographic applications. *IEEE J. Oceanic Engineering* (1992) **17** 288-291

[25] LEIGHTON TG, LINGARD RJ, WALTON AJ & FIELD JE. Acoustic bubble sizing by the combination of subharmonic emissions with an imaging frequency. *Ultrasonics* (1991) **29** 319-323

[26] PHELPS AD & LEIGHTON TG. Investigations into the use of two frequency excitation to accurately determine bubble sizes. *Proc. IUTAM Conf. on Bubble Dynamics and Interface Phenomena* (Birmingham 1993), ed. J. R. Blake et al., (1994) 475-483

[27] PHELPS AD & LEIGHTON TG. Acoustic bubble sizing using two frequency excitation techniques. *Proc. 2nd European Conf. on Underwater Acoustics* (Copenhagen 1994). ed. L. Bjorno. 1994, pp. 201 - 206

[28] LEIGHTON TG, PHELPS AD, RAMBLE DG & SHARPE DA. Comparison of the abilities of eight acoustic techniques to detect and size a single bubble. Submitted to *Ultrasonics*.

[29] LEIGHTON TG, SCHNEIDER M & WHITE PR. Study of dimensions of bubble fragmentation using optical and acoustic techniques. *Proc. Sea Surface Sound 1994* ed. M J Buckingham, J Potter Lake Arrowhead, California, March 1994. In press (1995)

[30] PHELPS AD, LEIGHTON TG, SCHNEIDER MF & WHITE PR. Acoustic bubble sizing, using active and passive techniques to compare ambient and entrained populations. ISVR Technical Report number 229, March 1994.

[31] PHELPS AD, LEIGHTON TG, SCHNEIDER MF, & WHITE PR. Active & passive acoustic bubble sizing. ISVR Technical Report 237, Oct. 1994.

[32] FEUILLADE C. Scattering from collective modes of air bubbles in water and the physical mechanism of superresonances. *JASA* (1995) **98** 1178-1190

[33] LEIGHTON TG, FAGAN KJ & FIELD JE. Acoustic and photographic studies of injected bubbles. *Eur. J. Phys.* (1991) **12** 77-85

[34] CLIFT R, GRACE JR, WEBER ME. Bubbles, Drops and Particles. Academic Press. 1978

[35] DEVIN C, Jr. Survey of Thermal, Radiation, and Viscous Damping of Pulsating Air Bubbles in Water. *JASA* (1959) **31** 1654